scientific reports

Check for updates

OPEN

Control of sensitivity in metal oxide electrolyte gated field-effect transistor-based glucose sensor by electronegativity modulation

Aeran Song[1], Min Jung Kim[1], Dong-Joon Yi[1], Soyeong Kwon[2], Dong-Wook Kim[2], Seunghwan Kim[3], Jee-Hwan Bae[3], Soohyung Park[3], You Seung Rim[4]✉, Kwang-Sik Jeong[5]✉ & Kwun-Bum Chung[1]✉

In this study, the sensitivity of electrolyte-gated field-effect transistor-based glucose sensors using oxide semiconductor materials was controlled via electronegativity modulation. By controlling the enzymatic reaction between glucose and glucose oxidase, which is affected by the surface potential, the sensitivity of the glucose sensor can be effectively adjusted. To evaluate the sensitivity characteristics of the glucose sensor according to electronegativity control, devices were fabricated based on InO through Ga and Zn doping. The results confirmed that the specific sensitivity range could be adjusted by increasing the electronegativity. In addition, density functional theory calculations, confirmed that the attachment energy of the surface-functionalized material and the enzyme binding energy in the surface-functionalized thin film can be modulated depending on the electronegativity difference. The dissociation constant was controlled in both directions by doping with metal cations with larger(Ga, 1.81) or smaller(Zn, 1.65) electronegativities in InO(In, 1.78). We expect that this study will provide a simple method for the gradual and bidirectional control of the glucose sensitivity region.

Keywords InO, InZnO, InGaO, Density functional theory (DFT), Glucose sensor, Electronegativity

Diabetes is a rapidly growing public health problem due to the exponential increase in obesity worldwide[1–3]. Glucose plays a key role in human metabolic processes, and abnormal glucose levels in the blood or body fluids are directly related to diabetes. Therefore, it is important for diabetics to constantly monitor their blood sugar levels (2–20 mM range)[4,5]. This monitoring involves performing a puncture test to extract blood, which can be painful[6]. The pain generated by this invasive method causes the patients to avoid self-control[7]. Therefore, much attention has been devoted to the noninvasive monitoring of continuous glucose levels. To replace this invasive method, which uses blood glucose, high sensitivity at low glucose concentrations is required, as the glucose concentration in body fluids such as tears (0.05–5 mM), saliva (0.008–1.77 mM), sweat (0.01–1.11 mM), and urine (0–0.8 mM) is much lower than in blood[8–11]. In addition, for long-term healthcare monitoring, selectivity, low cost, and high sensitivity tests should be considered[12,13].

Metal-oxide semiconductor field-effect transistors have recently received much attention as biosensors owing to their diverse merits, such as easy fabrication methods with solution processes or sputtering systems, good stability and chemical resistance, and easy surface functionalization. Therefore, metal-oxide semiconductor thin films are superior sensor materials for biochemical detection[14,15]. In particular, electrolyte-gated field-effect transistor (EGFETs)-based sensors using metal-oxide semiconductors such as InO[16], ZnO[17,18], Ta_2O_5-ZnO[19], and InGaZnO-FETs[1,20,21] have been intensively studied because of their advantages of stability in aqueous environments, operation at low driving voltages, and ability to convert and amplify biological signals into electronics[22]. In addition, research on glucose sensors using surface functionalization and/or enzymatic immobilization of metal-oxide thin films is actively being conducted. The advantages of non-enzymatic sensors

[1]Division of Physics and Semiconductor Science, Dongguk University, Seoul 100-715, Republic of Korea. [2]Department of Physics, Ewha Womans University, Seoul 03760, Republic of Korea. [3]Advanced Analysis and Data Center, Korea Institute of Science and Technology (KIST), Seoul 02792, Republic of Korea. [4]Department of Intelligent Mechatronics Engineering and Convergence Engineering for Intelligent Drone, Department of Semiconductor Systems Engineering, Sejong University, Seoul 05006, Republic of Korea. [5]Division of AI Semiconductor, Yonsei University, Wonju 26493, Republic of Korea. ✉email: youseung@sejong.ac.kr; JKS0701@yonsei.ac.kr; kbchung@dongguk.edu

include lower device fabrication costs and excellent stability. However, they suffer from low selectivity and interference from various compounds[23,24]. In contrast, when using enzymes, it is possible to operate at low voltages (< 0.6 V) and achieve high selectivity and specificity[25]. Glucose oxidase (GO_x) not only exhibits high selectivity for glucose targets but also withstands a wide range of pH and temperature conditions compared to other enzymes, making it the most common enzyme and a key component in numerous glucose biosensors[26]. According to several reports, enzymatic attachment to substances can be achieved using simple, convenient, and cost-effective methods[23,27]. Surface termination and enzyme immobilization according to surface functionalization vary depending on the oxide material and composition, and the surface mechanism changes accordingly. Previous studies[16–21] on glucose sensors using enzyme immobilization on the surface of oxide materials have confirmed the difference in glucose sensitivity characteristics depending on the selected oxide material, as well as the biosensor applicability of various oxide materials. Therefore, it is necessary to study the effect of the surface mechanism on surface termination and enzyme immobilization, as well as the correlation between its glucose sensor properties.

Therefore, we focused on the change in the surface state according to the electronegativity of the surface mechanism and investigated how the surface immobilization phenomenon according to the electronic structure of the metal oxide thin film affects the characteristics of the glucose sensor. To confirm the change in the surface mechanism depending on the surface conditions of the metal-oxide thin film, thin films and devices were fabricated by modulating the composition of the metal-oxide thin films by doping InO with Zn and Ga. Using these devices, the mechanism of the characteristic change of the glucose sensor was discovered, and experiments and theoretical calculations using density functional theory (DFT) confirmed that this mechanism is related to electronegativity.

Results

Surface characterization and morphology of the fabricated glucose sensors

Figure 1a shows the process flow of surface functionalization and enzyme immobilization on metal-oxide thin films using a solution process. Before the solution process, UV lamps (185 nm and 254 nm) were used on the thin film's surface for hydroxylation. For silanization, the samples were immersed in 4 wt% (3-aminopropyl) triethoxysilane (APTES) diluted with toluene. The samples were immediately rinsed with toluene to remove weakly bonded APTES molecules before the next step. After then 1.5 wt% glutaraldehyde (GD_x) was diluted with 1x PBS to cross-link the amine functional group between the surface of the silanized metal oxide thin films and the glucose oxidase (GO_x) molecules. Finally, the GO_x solution was added dropwise to the metal-oxide thin films over 24 h. A more detailed procedure is provided in the Experimental Section. To confirm the surface states before and after the surface functionalization, the morphologies of the InGaO, InO, and InZnO thin films were measured using scanning Atomic Force Microscopy (AFM) at a scan rate of 0.35 Hz. The three-dimensional (3D) topology images are shown in Fig. 1b. Each image measures 0.5 μm × 0.5 μm. After surface functionalization, the surface roughness R_q of the samples increased from 0.311, 0.322, and 0.326 to 1.70, 1.287, and 1.121 nm, respectively.

The structural properties of the InGaO, InO, and InZnO thin films were determined using high-angle annular dark field (HAADF) scanning transmission electron microscopy (STEM) images with energy dispersive spectroscopy (EDS) compositional mapping, and X-ray photoelectron spectroscopy (XPS) can be found in Fig. S1 and Table S1. The respective thicknesses of the InGaO, InO, and InZnO thin films were approximately 10.08, 13.77, and 9.84 nm, respectively, which are similar to the intended thickness (10 nm). In addition, STEM-EDS confirmed that approximately 10 nm of Si was present on the surfaces of the InGaO, InO, and InZnO thin films. For analysis, Pt was thinly deposited onto the thin-film surfaces. However, during this process, Pt penetrated the organic layer, affecting the appearance of the enzyme attached to the surface in the HAADF image and making it appear thinner. To confirm the presence or absence of elements and changes in the chemical binding states of the metal-oxide thin film surfaces as a result of surface functionalization and enzyme immobilization, as well as the amount of doped Zn and Ga, we used XPS analysis to measure the C, N, O, Si, In, Zn, and Ga spectra. Figure 1c shows the C 1s, N 1s, and O 1s XPS spectra of the InGaO, InO, and InZnO thin films before and after surface functionalization. The lowest binding energy O_I peak was located at 529.5 eV and can be attributed to the O^{2-} in the metal oxides, that is, In-O, Zn-O, and Ga-O. The O_{II} peak (531 eV) is related to the O^- in metal oxides. The highest binding energy O_{III} peak (532.5 eV) corresponds to the Si-O bonding states and/or electrolyte oxidation (APTES in Si, O, and O in metal oxides)[20,27,28]. Si and O were detected on all thin-film surfaces after surface functionalization, indicating that APTES adhered well to the thin-film surface, as shown in Fig. S2 and Table S2. In addition, C and N were detected in all thin films, indicating that they were well formed up to the last step of surface functionalization (Fig. 1d). Generally, all elemental spectra were calibrated using the standard binding energy of carbon, which is equal to 284.5 eV. The C 1*s* spectra were normalized and curve-fitted with five different Gaussian peaks to obtain the detailed chemical carbon bonding states, which were found to have low binding energies for C-C (284.5 eV), C-N and C = N (285.6 eV), C-O (286.5 eV), and C = O (287.7 eV), and high COO binding energies (288.5 eV)[29]. The C 1s peak was assigned to the C-N and C = N bonds (285.6 eV), confirming the combination of GDx with GOx on each surface of the metal oxide thin film. When Ga and Zn were mixed into the InO material, the relative chemical bonding states of the C-N peaks increased. The N 1s spectra were normalized and curve-fitted using three different Gaussian peaks of the detailed chemical bonding states of nitrogen, which included peaks corresponding to low binding energy (C = N; 398.6 ± 0.1 eV), medium energy (C-N and $(Si-)_2$N-O; 399.6 eV), and high energy ($C-N^+$; 400.7 ± 0.1 eV)[7,30,31]. Detailed information on the fitting results is provided in Table S2. The ratios of neutral amine nitrogen (C-N and $(Si-)_2$N-O) to positively charged protonated amine nitrogen ($C-N^+$) decreased to 1:0.18, 1:0.16, and 1:0.15 as the electronegativity decreased. A high percentage of $C-N^+$ means that the enzyme is better able to bind to the functionalizing substance[7,31]. This appeared to follow an electronegativity trend.

Figure 1

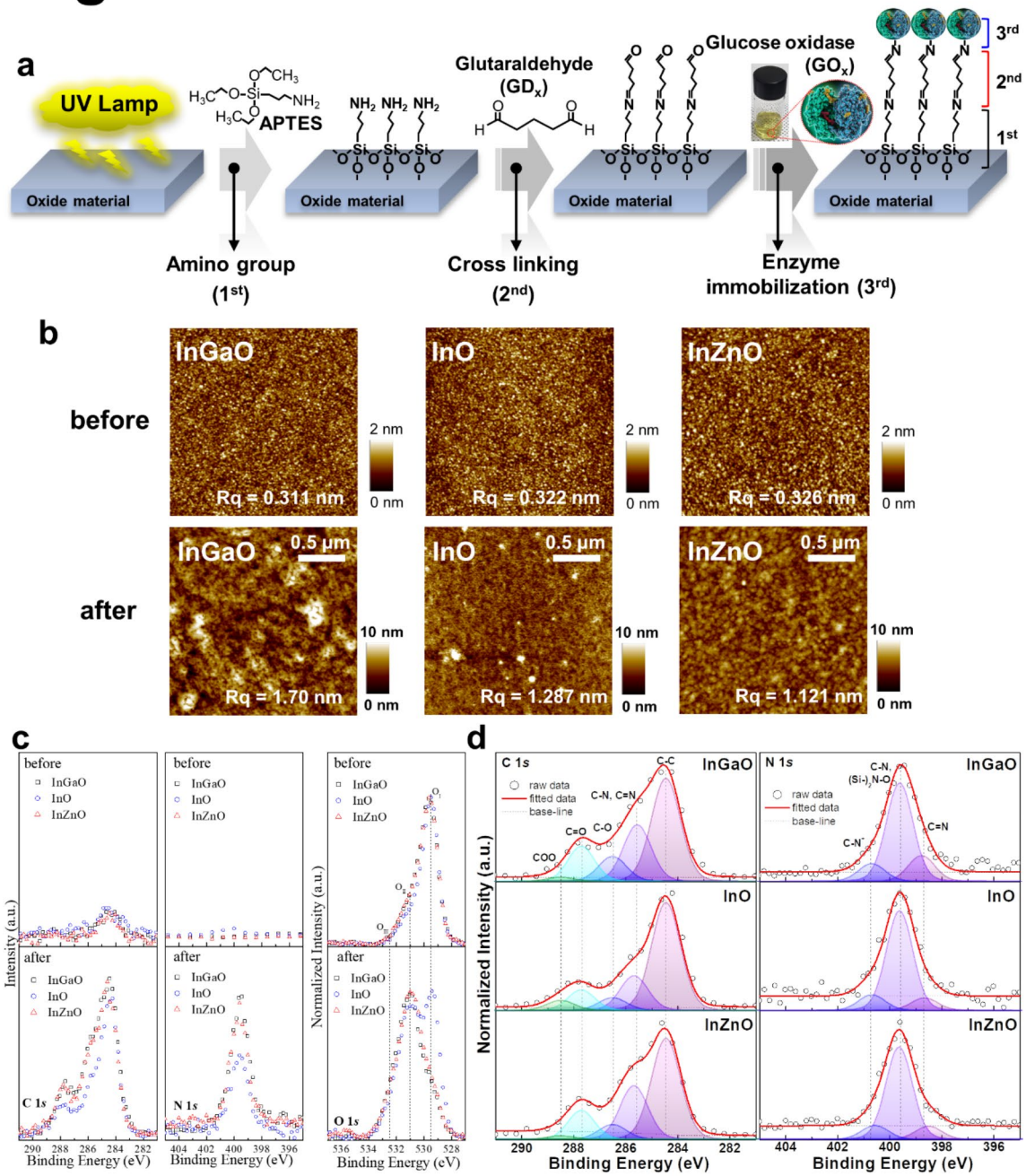

Fig. 1. (**a**) Scheme of surface functionalization (**b**) Topologies of the InGaO, InO, and InZnO thin films before and after surface functionalization. (**c**) C 1s, N 1s, and O 1s XPS spectra of InGaO, InO, and InZnO thin films before and after surface functionalization. (**d**) XPS spectra showing the deconvolution of C 1s and N 1s of the surface-functionalized InGaO, InO, and InZnO thin films.

Electrochemical characterization of fabricated glucose sensors

Figure 2a shows diagrams and photographs of the fabricated metal-oxide EGFET-based glucose sensor devices. The devices were operated in 1× PBS, and a commercially available leak-free Ag/AgCl reference electrode placed over the sensing area was used as the floating gate. A PDMS wall was used on top of the exposed metal oxide channel to define the sensing area and contain the electrolyte.

The electrical characteristics of the device measured in the 1× PBS solution differed from those measured in air, as shown in Fig. 2b and c. In particular, the Ion/off ratio obtained in the air state had a value of approximately 10^7 to 10^8 at a drain voltage of 5 V and gate voltage in the range of -30–30 V. The transfer curves of each device indicate that we obtained high field effect mobilities (μ_{FET}) of 16.81, 17.89, and 9.15 cm^2/Vs, respectively, in air. The threshold voltage (V_{th}) was calculated to be -2.15, -8.18, and − 1.08 V, respectively. On the other hand, the value obtained under 1× PBS solution was lower, ranging from 10^4 to 10^5 at a drain voltage of 0.1 V and gate voltage in the range of -0.5–0.5 V. This is related to the ionic strength of the 1× PBS solution and the low applied voltage. A comprehensive study was conducted by Kim et al.1 to investigate and analyze the effects of solvents on metal-oxide TFTs. The results of the study indicate that the solvent predominantly affects other donor-like defects, such as hydrogen donors and metal interstitials, or the change in deep traps originating from metal vacancies rather than oxygen vacancies as shallow donors. However, this is not a low (or poor) value for driving the device, and the sensitivity characteristics can be evaluated according to the molarity of glucose. Furthermore, as shown in Table 1, the device operation characteristics in the air and solution states fabricated by the sputtering system are superior, even when compared to the characteristics presented in previous papers. The transfer curves of each device indicate that they have high on/off ratios ($> 10^4$) and we obtained high field effect mobilities (μ_{FET}) of 8.7, 15.1, and 8.5 cm^2/Vs, respectively, in 1× PBS. The subthreshold gate swing (SS) and threshold voltage (V_{th}) were calculated to be 40, 30, and 30 mV/dec. and 0.01, 0.06, and 0.03 V, respectively. The reproducibility of each device characteristic was excellent, and the results are shown in Fig. S3 and Table S3. The SS is an important parameter for these devices because it provides a gating effect deficiency and biosensor sensitivity[13,28,32]. The biosensor sensitivity is extremely high in the SS region owing to greater current changes, which is known as the gating effect owing to proton variation[33]. Therefore, to achieve optimal sensing performance, the devices were controlled by an Ag/AgCl reference electrode to tune their operating point to the SS regime. The mechanism of enzyme-based biosensors involves recognizing a biochemical reaction by attaching a recognition element to the device. Glucose detection is a representative application of enzyme-based sensors and byproducts in which the oxidation or reduction of the targets affects the electrical properties of the sensors. The structure used in this study is easy to fabricate, and the channel layer, which is exposed to the outside environment, can react more sensitively with biomolecules. An illustration of the glucose detection mechanism is presented in S4. Real-time measurements were performed according to changes in glucose concentration to determine the effect of differences in surface functionalization and enzyme imm obilization on the glucose detection characteristics, depending on the metal-oxide material used in the device. The enzymatic reactions between glucose and GOx are as follows[9,34]:

$$\begin{gathered} D-glucose+O_2+H_2O \;\rightarrow\; D-gluconicacid+H_2O_2+H^+ \\ GO_x \\ 2H^++O_2+2e^- \;\leftarrow\; H_2O_2 \end{gathered} \tag{1}$$

GO_x catalyzes the conversion of glucose to gluconic acid and hydrogen peroxide (H_2O_2), which in turn react to form proton ions and electrons[35]. As the glucose concentration reacts with the GO_x, the concentration of protons in the electrolyte increases. An increase in the proton concentration can control the charge in the channel layer of a metal-oxide EGFET-based glucose sensor device and amplify the current. The solution at each glucose concentration (~ 0.25μL) was injected into the PDMS wall (~ 100μL) using a micropipette. The glucose concentration was varied from 0 to 4 mM, corresponding to the tear (0.1–0.4 mM), urine (0–0.8 mM), sweat (0.01–1.11 mM), and saliva (8 μM–1.77 mM) glucose levels of diabetic patients. To quantify the sensor's response to glucose, the real-time measurement results according to the glucose concentration, as shown in S5, were converted into the sensor's response voltage change and the calibrated response voltage according to the glucose concentration (Fig. 3a and b).

The ΔV_{on} plot according to glucose concentration is consistent with the Hill-Langmuir equation[36] for equilibrium ligand-receptor binding:

$$V_{on} \;=\; \Delta V_{on,\,max}\frac{(\frac{c}{K_d})^n}{1+(\frac{c}{K_d})^n}+\Delta V_{on,pristine} \tag{2}$$

where c is the glucose concentration, K_d is the dissociation constant of gluconic acid-glucose interaction, n is the Hill coefficient describing the cooperativity of the binding, $\Delta V_{on,\,max}$ is the V_{on} shift when gluconic acid molecules are bound to glucose[37], and $\Delta V_{on,\,pristine}$ is the V_{on} in 1× PBS. As the electronegativity value decreased, the dissociation constants for the InGaO, InO, and InZnO EGFET-based glucose sensor devices increased to 0.15, 0.62, and 2.49 mM, respectively, and the glucose concentration corresponding to the highest calibrated response voltage value also increased.

By evaluating the transfer curve characteristics according to the glucose concentration, the calibrated response voltage was obtained using the following formula:

$$\text{Calibrated response Voltage} \;=\; \mathrm{DI}/(\mathrm{DI_{ds}}/\mathrm{DV_{gs}}),$$

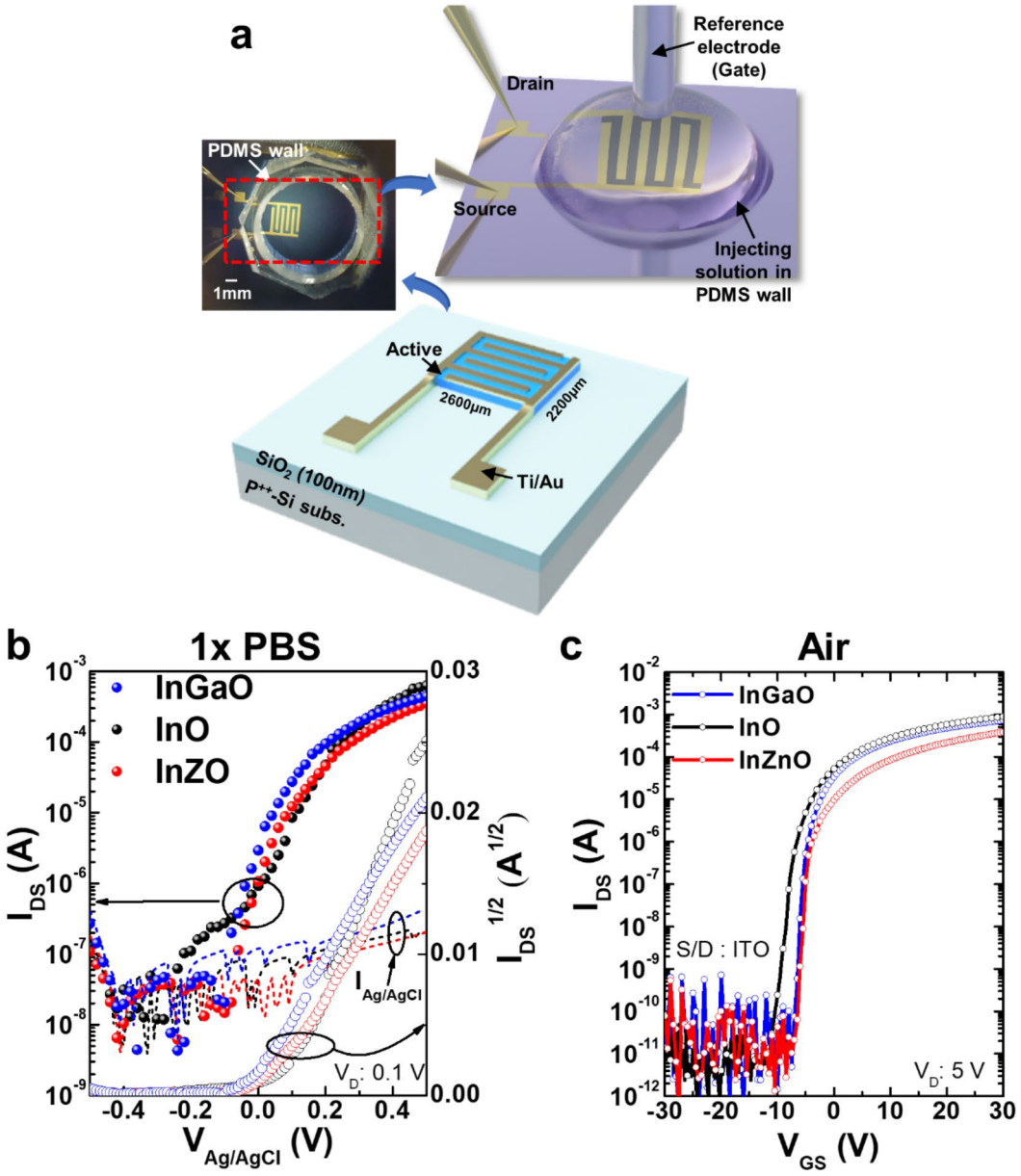

Fig. 2. (**a**) Diagram of the fabricated metal-oxide EGFETs-based glucose sensor device. The inset image shows a top view of the attached PDMS wall and the sensing method. (**b**) Characteristics of the transfer curves (I_{DS}-V_{GS}, Ag/AgCl) of InGaO (blue circle), InO (black circle), and InZnO (red circle) EGFETs-based devices in 1× PBS solution. (**c**) Characteristics of the transfer curves (I_{DS}-V_{GS}) of InGaO (blue circle), InO (black circle), and InZnO (red circle) devices in air.

Materials	FM	Thickness (nm)	Electrical properties of FET based biosensors						Sensing properties of GOx based biosensors				
			In air			In solution							
			V_D (V)	$I_{on/off}$	S.S (mV/dec.)	V_D (V)	$I_{on/off}$	S.S (mV/dec.)	Sol.	K_d (M)	DR (M)	DL (M)	RE
This work													
InGaO	SPT	10	5.00	4.09×10^7	480	0.10 (1xPBS)	$\sim10^5$	40	1× PBS	0.15 m	0.1–1 m	100µ	Ag/AgCl
InO			5.00	1.21×10^8	600	0.10 (1xPBS)	1.69×10^4	30		0.62 m	0.05–2 m	50µ	
InZnO			5.00	3.18×10^7	470	0.10 (1xPBS)	1.34×10^4	30		2.49 m	0.2–4 m	2 m	
IGZO[1]	SPT	100				nr			1× PBS	nr	5µ − 1 m	nr	nr
Ta_2O_5/ZnO: In[19]	SPT	8/35				nr			5mM PBS	nr	3–280 m	3 m	Ag/AgCl
IGZO[20]	SPT	50	0.10	$\sim10^5$	nr	0.10 (PBS)	$\sim10^3$	nr	160mM PBS	nr	up to 28 m	nr	Ag/AgCl
IGZO[21]	SPT	50				0.30 (1xPBS)	$\sim10^4$	38	1× PBS	nr	0.05–2 m	5µ	Ag/AgCl
In_2O_3[16]	SC	3.5	nr	$\sim10^8$	580	0.25 (PBS)	$<10^4$	nr	1× PBS	nr	0.1–0.6 m	nr	Ag/AgCl
ZnO NR[17]	Sol.	1 µm				nr			10mM PBS	nr	0.01–5 m	3.8µ	Ag/AgCl
ZnO NR[18]	NJP	600				nr			100mM PBS	nr	0–80 m	70µ	Ag/AgCl

Table 1. Comparison of electrical and glucose sensing properties of FETs composed of different metal oxides. Fabrication method: FM, Sputtering: SPT, Spin coating: SC, Solution: Sol., Nozzle-jet printing: NJP, Dissociation constant of gluconic acid-glucose interaction: K_d, glucose oxidase: GOx, detection range: DR, detection limit: DL, reference electrode: RE, phosphate buffered saline: PBS, ZnO nanoribbon: ZnO NR, indium-gallium-zinc-oxide: IGZO.

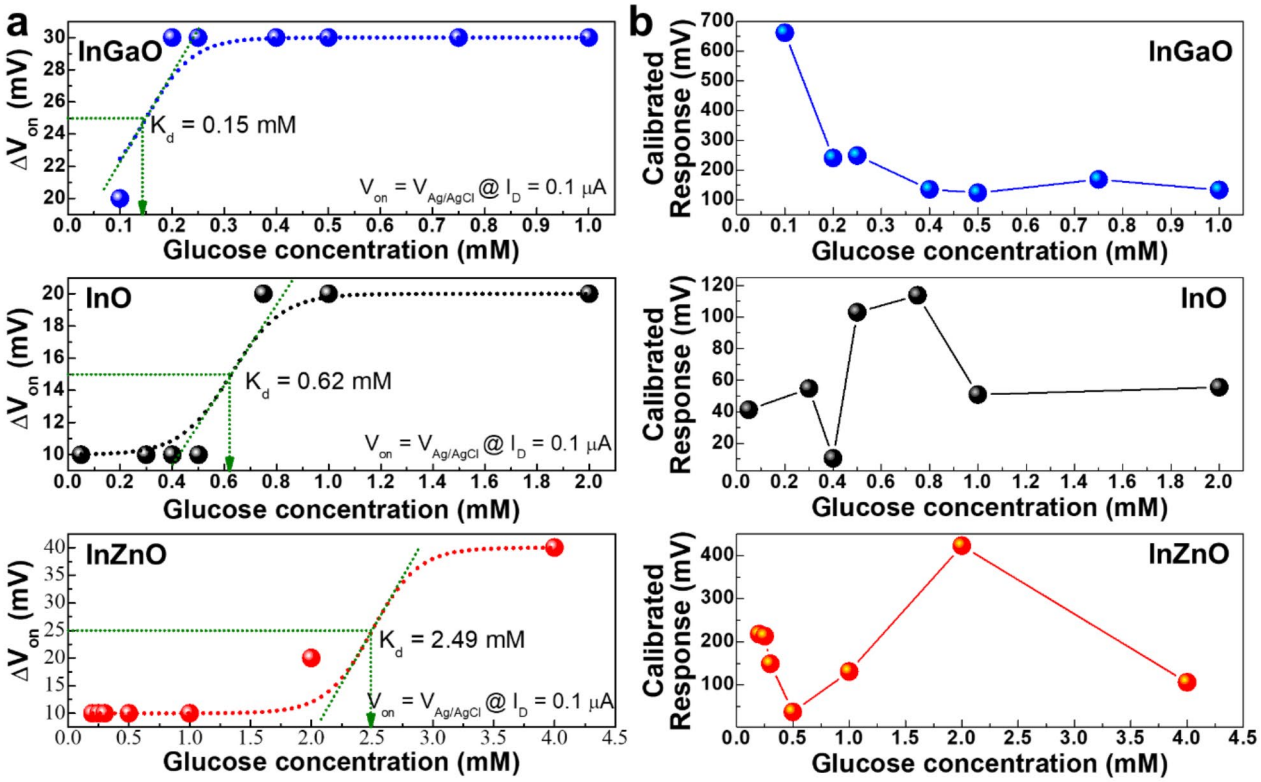

Fig. 3. (**a**) Response voltage and (**b**) calibrated response voltage according to glucose concentration of the InGaO, InO, and InZnO EGFET-based devices in 1× PBS.

$$DI = I_{DS,\ \text{according to glucose concentration}} - I_{0,\ \text{w/o glucose, only PBS solution}}$$

To assess its stability, the InO-based glucose sensor was subjected to additional testing using glucose titration at different intervals, as shown in S6. Although the response decreased slightly after the initial period, the relative sensitivity of the glucose sensor remained at a minimum of 94% during the first 10 d, similar to a previously published paper[38]. These results demonstrate that the glucose sensor can maintain a stable state over an extended period.

Table 1 shows the properties of the InGaO, InO, and InZnO EGFET-based glucose sensor devices compared with those of previously reported metal-oxide EGFET-based devices. The minimum detection range of the three samples was lower than that of the others, even for 1× PBS, which is a high-ionic-strength electrolyte[39]. The glucose concentration in different body secretions varies, offering choices for detecting glucose concentrations using specific secretions. The sensing characteristics of the InGaO (0.15 mM), InO (0.62 mM), and InZnO (2.49 mM) EGFET-based glucose sensors are comparable to those of other sensors that can detect glucose at very low concentrations in tears, urine, and sweat. Considering the constant dissociation characteristics of InGaO, InO, and InZnO, InGaO has the potential for use in sensors measuring the glucose concentration in tears, whose glucose concentration is relatively lower than that of other bodily secretions. InO appears to have the potential for use in sensors using urine or sweat, and InZnO may be applied to sensors using saliva or ISF. Therefore, materials that can react more sensitively to the concentration of glucose (specific region) in a specific detection substance can be selected. However, if devices with different compositions are used in parallel (such as devices using the materials introduced in this paper, that is, InO, InGaO, and InZnO), the linearity of the components can be achieved in a much broader range of areas. To confirm the effect of the electronegativity change caused

by doping InO with Ga or Zn, we predicted the formation energies of surface functionalization and enzyme immobilization.

Theoretical calculations of the density functional theory by surface of glucose sensor

The reaction energy diagrams for functionalization and enzyme immobilization are shown in Fig. 4. Owing to the large size of GOx (Aspergillus niger), we consider H-NH_2 as GOx-NH_2. In the first functionalization process, In(Ga/Zn)O was surface-hydroxylated by UV, and the surface was partially terminated with OH. These OH groups reacted with the C_2H_5 group from APTES, and APTES was attached to the In(Ga/Zn)O surface. Through cross-linking, the APTES-GDx chains were synthesized and terminated via C=O bonding. In the functionalization process, Ga doping (increasing electronegativity) decreased the sensitive formation energy at each step, whereas Zn doping (decreasing electronegativity) increased the formation energy at each step. Similar to the functionalization process, the formation energy of enzyme immobilization can be controlled by doping with Ga or Zn. At the end of the GDx, which is terminated by a C=O bond, GOx is immobilized to form a C=N-GOx (C=N-H by DFT calculations) bond. With Ga doping, the formation energy of immobilization becomes more negative than that of InO, whereas with Zn doping, the energy of immobilization becomes more positive than that of InO. Therefore, the amount of functionalized surface or immobilized enzyme should be in the order InZnO < InO < InGaO, which corresponds to the surface roughness and the number of N-N + bonds in XPS. As a control amount of GOx by Zn or Ga doping, the frequency of the reaction of d-glucose to glucose acid, as well as the concentration of glucose to which the oxide sensor responds (that is, becomes more sensitive or insensitive by Ga or Zn doping), can be modulated.

Discussion

In this study, we induced changes in the surface termination of metal-oxide thin films by controlling their electronegativity using a sputtering deposition system. XPS analysis confirmed that the surface functionalization states of the modified thin films were different. The adhesion energy of the surface-functionalized material and the enzyme immobilization binding energy of the surface-functionalized thin film were calculated by DFT, and their glucose detection characteristics were evaluated. A difference in the amount of surface functionalization can change the material's binding energy with glucose, resulting in a difference in the amount of charge it holds, thus indicating that the chemical potential energy of the attached glucose can be controlled. As the electronegativity increased, the percentage of positively charged protonated amine nitrogen (C-N^+) increased, indicating that the binding of the enzyme to the functionalizing substance improved. In addition, a reduction

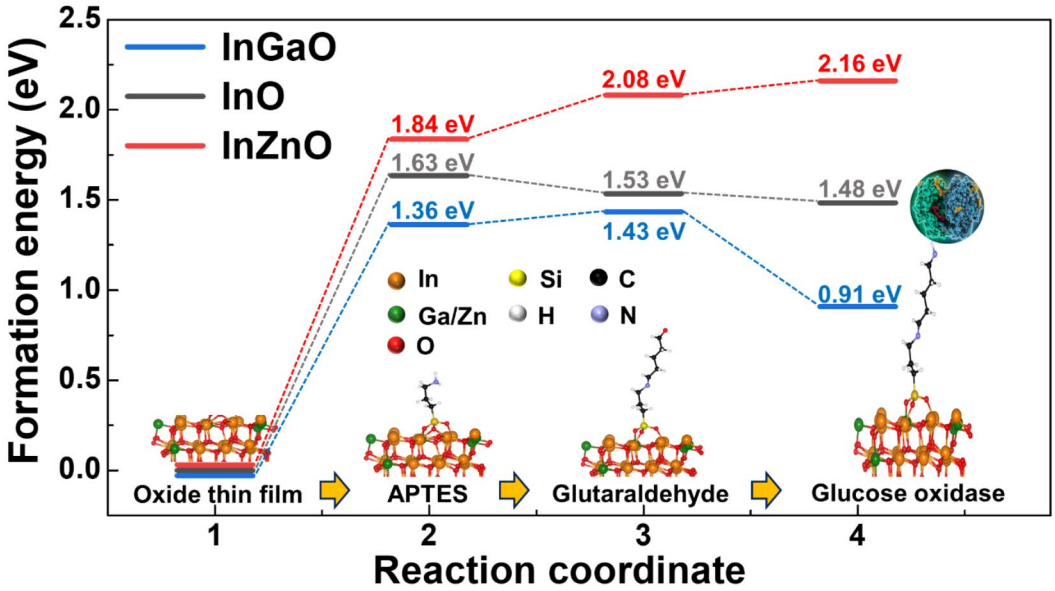

Fig. 4. Reaction energy diagram at 0 eV (Ref.; InO) for the immobilization of the glucose oxidase (GO_x) enzyme in three different samples.

in the formation energy for surface functionalization and enzyme immobilization resulted in a decrease in the dissociation constant. The sensitivity region of the glucose sensor could be adjusted by electronegativity control, and InGaO, InO, and InZnO exhibited differences in the most sensitive response regions at 0.15, 0.62, and 2.49 mM, respectively.

Therefore, materials that can react more sensitively to the concentration of glucose (specific region) present in a specific detection substance may be selected. In addition, the performance of glucose monitoring devices using these materials is comparable to that of devices fabricated using not only the sputtering system but also the spin coating, solution, and printing systems. To achieve practical applications and scalability of oxide-semiconductor-based biosensors, precise process control is crucial, and this can be implemented using a vacuum system. This study represents a milestone in the design of biomaterials. Furthermore, if devices with different compositions are used in parallel (such as those using materials introduced in this paper, that is, InO, InGaO, and InZnO), the linearity of the components can be achieved in a much broader range of areas.

Materials and methods

Device fabrication

The thermally grown 100-nm-thick silicon dioxide (SiO_2) layer on a heavily doped p-type silicon (p^{++}-Si) substrate was cleaned with acetone, ethanol, and DI water in a sonicator. After cleaning the substrate, the first shadow metal mask was attached to define the active channel layer. Then, a 10-nm-thick InO layer was deposited using a DC sputtering system with a 3-inch In_2O_3 (99.995%, 4N5) target at a power of 30 W without substrate temperature. After deposition, interdigitated Ti 30 nm (bottom) and Au 200 nm (top) electrodes were deposited using a thermal evaporation system. The source and drain areas were defined using a second shadow metal mask during electrode deposition. The fabricated channel width (W) and length (L) of the device were 10,200/200 μm, respectively. Finally, the InO EGFETs were annealed in a quartz tube furnace at 250 ℃ in air for 1 h to modify the stoichiometry of the films.

The fabrication methods for the InZnO and InGaO EGFETs were almost the same as those for the InO EGFETs, except for the co-sputtering method used in the deposition process of the active channel layer. Two 10-nm-thick InZnO EGFETs were fabricated, one using the co-sputtering of a 3-inch ZnO target (99.999%, 5 N, RF) at a power of 20 W and another using the co-sputtering of a 3-inch In2O3 target (99.995%, 4N5, DC) at a power of 30 W. Two 10-nm-thick InGaO EGFETs were fabricated, one using the co-sputtering of a 3-inch Ga_2O_3 target (99.99%, 4 N, RF) at a power of 20 W and another using the co-sputtering of a 3-inch In_2O_3 target at a power of 30 W without substrate temperature. The conditions used for the fabrication of all thin films were the same. The reactive gas flow rate ratio was Ar: O_2 = 19:0.5 (O_2 = 2.6%), and the working pressure of the main chamber was 5 mTorr.

Preparation of surface functionalization

InO-, InZnO-, and InGaO-FETs were UV-treated in air for 10 min before surface functionalization. The samples were modified stepwise for glucose detection. First, (3-aminopropyl)triethoxysilane (APTES, Sigma-Aldrich) was self-assembled on the surface of each device using 4 wt% APTES in toluene (Sigma-Aldrich) for 20 min. The samples were then directly rinsed with toluene. Next, the silanized samples were immersed in a 1.5 wt% glutaraldehyde linker (GDx, Sigma-Aldrich) in phosphate-buffered saline (1× PBS with pH 7.4, Sigma-Aldrich) solution for 5 min. The samples were immediately rinsed with 1× PBS. Next, 3 mg of glucose oxidase (GOx) from Aspergillus niger (Sigma-Aldrich) was immobilized on the APTES-GDx-treated surfaces in 6 ml of 1× PBS solution for 24 h. The samples were rinsed with 1× PBS. Finally, to protect the Au electrode from the electrolyte environment containing 1-dodecaneethiol (DDSH), the sample was treated with 1 wt% 1-DDSH in ethanol (99.99%, 4 N) for 1 h. All steps for surface functionalization were carried out at room temperature. The samples were then rinsed with ethanol. D-glucose (Sigma-Aldrich) was dissolved in 1× PBS at different concentrations.

Glucose detection

The electrical characteristics and glucose-sensing performance of all the metal-oxide-semiconductor EGFET-based glucose sensors were evaluated at room temperature using a Keithley SCS-4200 semiconductor parameter analyzer and an Ag/AgCl leak-free reference electrode (LF-1, DONGWOO Science Co., Ltd.) in an electrolyte gate environment. For the evaluation of transistor's performance, the transconductance (g_m) of the metal oxide EGTFTs were calculated from an I_D–$V_{Ag/AgCl}$ curve using the following equation:

$$g_m = dI_D/dV_{Ag/AgCl} = W/L\ (C_{DL}m_{FE}V_D)$$

where W is the channel width, L is the channel length, and C_{DL} is the electrical double layer capacitance per unit area in 0.1 M ionic strength aqueous solution reported previously (25.52 μF cm^{-2})[16]. A comprehensive study was conducted Park et al.[40] to investigate electrical double layer capacitance per unit area of metal oxide EGTFTs under various aqueous dielectric conditions. A polydimethylsiloxane (PDMS) solution was attached to the top of the device to determine the contact area of the analyte solution during the detection test according to the glucose concentration. The transfer curve characteristics (I_{DS}-V_{GS}) were measured at a fixed drain-to-source voltage (V_{DS}) of 0.1 V. A low V_{DS} was used to minimize electrochemical reactions that could occur when the source and drain electrodes come into contact with the analyte solution[12]. The sensitivity characteristics of metal-oxide-semiconductor EGFET-based glucose sensors according to glucose concentration were evaluated in real time in the following order. 1st 1x PBS (0.25μL) into the PDMS → measurement → removal of 1x PBS (0.25μL) from PDMS. 2nd Glucose mole concentration (0.25μL) into the PDMS → glucose detection → removal of glucose mole concentration (0.25μL) from PDMS → 1x PBS (0.25μL) into the PDMS to rinse for a few seconds. From the second step, it was performed repeatedly according to the change in glucose molar concentration.

Characterizations of thin films

Atomic Force Microscopy (AFM, Park Systems, NX10) was performed in an N_2-purging glove box to minimize surface contamination and confirm the thin film's topography. The chemical bonding states were determined by X-ray photoelectron spectroscopy (XPS) using a monochromatic Al Kα source with a pass energy of 29.35 eV. The XPS spectra were measured after eliminating the surface contamination caused by the adsorption of OH, C, H2O, etc., using Ar + ions at 500 eV. Transmission electron microscopy (TEM) images were obtained using a Talos F200X (FEI) equipped with an EDS (Bruker). The thickness of InGaO, InO, and InZnO thin films was determined using high-angle annular dark field (HAADF)-scanning transmission electron microscopy (STEM) images.

Calculations of the density functional theory

DFT calculations were performed using the Vienna Ab initio Simulation Package (VASP) with PBEsol functionality[41–43]. First, the bulk unit cell of cubic In_2O_3 was geometrically optimized with 3 × 3 × 3 K points and a cutoff energy of 500 eV until the condition of 0.02 eV/Å was met. Using the optimized bulk structure, we generated a (111) surface model with the lowest surface energy[44]. To minimize slab-to-slab interactions, a 50-Å slab of vacuum was inserted between the In_2O_3 layers. The various molecules related to functionalization and immobilization processes were attached to the In_2O_3 (111) surfaces, and the geometry was optimized using 3 × 3 × 1 K points and a cutoff energy of 500 eV until the 0.1 eV/Å condition was met. For the optimized structure, the total energies with 3 × 3 × 1 K points and a cutoff energy of 500 eV were predicted to calculate the formation energy of the reaction. To evaluate the effect of Ga/Zn doping, we randomly replaced 10% of In in the Ga or Zn system, optimized the geometry, and calculated the total energies under the same conditions as for In_2O_3.

Data availability

The datasets used and/or analysed during the current study available from the corresponding author on reasonable request. Correspondence and requests for materials should be addressed to K.-B. Chung, K.-S. Jeong, or Y. S. Rim (email: kbchung@dongguk.edu; JKS0701@yonsei.ac.kr; youseung@sejong.ac.kr).

Received: 7 July 2024; Accepted: 17 October 2024
Published online: 08 November 2024

References

1. Kim, H. & Kwon, J. Y. Enzyme immobilization on metal oxide semiconductors exploiting amine functionalized layer. *RSC Adv.* **7**, 19656–19661 (2017).
2. Yoo, E. H. & Lee, S. Y. Glucose biosensors: an overview of use in clinical practice. *Sens. (Basel).* **10**, 4558–4576 (2010).
3. So, C. F., Choi, K. S., Wong, T. K. S. & Chung, J. W. Y. Recent advances in noninvasive glucose monitoring. *Med. Devices (Auckl).* **5**, 45–52 (2012).
4. Pambianco, G. et al. The 30-year natural history of type 1 diabetes complications: the Pittsburgh epidemiology of diabetes complications study experience. *Diabetes*. **55**, 1463–1469 (2006).
5. Nathan, D. M. The diabetes control and complications trial/epidemiology of diabetes interventions and complications study at 30 years: overview. *Diabetes Care*. **37**, 9–16 (2014).
6. Strakosas, X. et al. A non-enzymatic glucose sensor enabled by bioelectronic pH control. *Sci. Rep.* **9**, 10844 (2019).
7. Toghill, K. E. & Compton, R. G. Electrochemical non-enzymatic glucose sensors: a perspective and an evaluation. *Int. J. Electrochem. Sci.* **5**, 1246–1301 (2010).
8. Lee, H., Hong, Y. J., Baik, S., Hyeon, T. & Kim, D. H. Enzyme-based glucose sensor: from invasive to wearable device. *Adv. Healthc. Mater.* **7**, e1701150 (2018).
9. Bruen, D., Delaney, C., Florea, L. & Diamond, D. Glucose sensing for diabetes monitoring: recent developments. *Sensors*. **17**, 1866 (2017).
10. Claussen, J. C. et al. Nano structuring platinum nanoparticles on multilayered graphene petal nanosheets for electrochemical biosensing. *Adv. Funct. Mater.* **22**, 3399–3405 (2012).
11. Makaram, P., Owens, D. & Aceros, J. Trends in nanomaterial-based non-invasive diabetes sensing technologies. *Diagnostics (Basel).* **4**, 27–46 (2014).
12. Vu, C. A. & Chen, W. Y. Field-effect transistor biosensors for biomedical applications: recent advances and future prospects. *Sens. (Basel).* **19**, 4214 (2019).
13. Zhang, H. et al. Graphene-enabled wearable sensors for healthcare monitoring. *Biosens. Bioelectron.* **197**, 113777 (2022).
14. Liu, N., Chen, R. & Wan, Q. Recent advances in electric-double-layer transistors for bio-chemical sensing applications. *Sens. (Basel).* **19**, 3425 (2019).
15. Rim, Y. S. Review of metal oxide semiconductors-based thin-film transistors for point-of-care sensor applications. *J. Inf. Disp.* **21**, 203–210 (2020).
16. Rim, Y. S. et al. Printable ultrathin metal oxide semiconductor-based conformal biosensors. *ACS Nano*. **9**, 12174–12181 (2015).
17. Fathollahzadeh, M. et al. Immobilization of glucose oxidase on ZnO nanorods decorated electrolyte-gated field effect transistor for glucose detection. *J. Solid State Electrochem.* 22, 61–67 (2018).
18. Bhat, K. S., Ahmad, R., Yoo, J. Y. & Hahn, Y. B. Nozzle-jet printed flexible field-effect transistor biosensor for high performance glucose detection. *J. Colloid Interface Sci.* **506**, 188–196 (2017).
19. Yano, M. et al. Zinc oxide ion-sensitive field-effect transistors and biosensors. *Phys. Status Solidi A*. **211**, 2098–2104 (2014).
20. Du, X., Li, Y., Motley, J. R., Stickle, W. F. & Herman, G. S. Glucose sensing using functionalized amorphous in – Ga – Zn – O field-effect transistors. *ACS Appl. Mater. Interfaces*. **8**, 7631–7637 (2016).
21. Kim, H., Rim, Y. S. & Kwon, J. Y. Evaluation of metal oxide thin-film electrolyte-gated field effect transistors for glucose monitoring in small volume of body analytes. *IEEE Sens. J.* **20**, 9004–9010 (2020).
22. Kim, Y. G. et al. Facile fabrication of wire-type indium gallium zinc oxide thin-film transistors applicable to ultrasensitive flexible sensors. *Sci. Rep.* **8**, 5546 (2018).
23. Mohamad Nor, N., Ridhuan, N. S. & Abdul Razak, K. Progress of enzymatic and non-enzymatic electrochemical glucose biosensor based on nanomaterial-modified electrode. *Biosensors*. **12**, 1136 (2022).
24. Naikoo, G. A. et al. Recent advances in non-enzymatic glucose sensors based on metal and metal oxide nanostructures for diabetes management-a review. *Front. Chem.* **9**, 748957 (2021).

25. Bollella, P., Gorton, L., Ludwig, R. & Antiochia, R. A third generation glucose biosensor based on cellobiose dehydrogenase immobilized on a glassy carbon electrode decorated with electrodeposited gold nanoparticles: characterization and application in human saliva. *Sens. (Basel)*. **17**, 1912 (2017).
26. Teymourian, H., Barfidokht, A. & Wang, J. Electrochemical glucose sensors in diabetes management: an updated review (2010–2020). *Chem. Soc. Rev.* **49**, 7671–7709 (2020).
27. Lipińska, W. et al. The optimization of enzyme immobilization at Au-Ti nanotextured platform and its impact onto the response towards glucose in neutral media. *Mater. Res. Express*. **6**, 1150e3 (2019).
28. Sarkar, D. & Banerjee, K. Proposal for tunnel-field-effect-transistor as ultra-sensitive and label-free biosensors. *Appl. Phys. Lett.* **100**, 143108 (2012).
29. Desimoni, E. & Brunetti, B. X-ray photoelectron spectroscopic characterization of chemically modified electrodes used as chemical sensors and biosensors: a review. *Chemosensors*. **3**, 70–117 (2015).
30. Major, G. H. et al. Practical guide for curve fitting in x-ray photoelectron spectroscopy. *J. Vac Sci. Technol. A*. **38**, 061203 (2020).
31. BaO, S. J., Wang, Y., Wei, Z., Yang, W. & Yu, Y. Highly efficient recovery of heavy rare earth elements by using an amino-functionalized magnetic graphene oxide with acid and base resistance. *Hazard. Mater.* **424**, 127370 (2022).
32. Li, B. R., Chen, C. C., Kumar, U. R. & Chen Y.-T. Advances in nanowire transistors for biological analysis and cellular investigation. *Analyst*. **139**, 1589–1608 (2014).
33. Gao, X. P. A., Zheng, G. & Lieber, C. M. Subthreshold regime has the optimal sensitivity for nanowire FET biosensors. *Nano Lett.* **10**, 547–552 (2010).
34. Yoon, H., Ko, S. & Jang, J. Field-effect-transistor sensor based on enzyme-functionalized polypyrrole nanotubes for glucose detection. *J. Phys. Chem. B*. **112**, 9992–9997 (2008).
35. Kang, B. C., Park, B. S., Ha, T. J. & Ha & T.-J. highly sensitive wearable glucose sensor systems based on functionalized single-wall carbon nanotubes with glucose oxidase-nafion composites. *Appl. Surf. Sci.* **470**, 13–18 (2019).
36. Hill, A. V. A new mathematical treatment of changes of ionic concentration in muscle and nerve under the action of electric currents, with a theory as to their mode of excitation. *J. Physiol.* **40**, 190–224 (1910).
37. Chen, H. et al. Quasi-two-dimensional metal oxide semiconductors based ultrasensitive potentiometric biosensors. *ACS Nano*. **11**, 4710–4718 (2017).
38. Huang, L., Jia, Z., Liu, H., Pi, X. & Zhou, J. Design of a sandwich hierarchically porous membrane with oxygen supplement function for implantable glucose sensor. *Appl. Sci.* **10**, 2848 (2020).
39. Palazzo, G. et al. Detection beyond Debye's length with an electrolyte-gated organic field-effect transistor. *Adv. Mater.* **27**, 911–916 (2015).
40. Park, S. Sub-0.5 V highly stable aqueous salt gated Metal Oxide Electronics. *Sci. Rep.* **5**, 13088 (2015).
41. Kresse, G. & Furthmüller, J. Efficiency of ab-initio total energy calculations for metals and semiconductors using a plane-wave basis set. *Comput. Mater. Sci.* **6**, 15–50 (1996).
42. Kresse, G. & Joubert, D. From ultrasoft pseudopotentials to the projector augmented-wave method. *Phys. Rev. B*. **59**, 1758–1775 (1999).
43. Perdew, J. P. et al. Restoring the density-gradient expansion for exchange in solids and surfaces. *Phys. Rev. Lett.* **100**, 136406 (2008).
44. Walsh, A. & Catlow, C. R. A. Structure, stability and work functions of the low index surfaces of pure indium oxide and Sn-doped indium oxide (ITO) from density functional theory. *J. Mater. Chem.* **20**, 10438–10444 (2010).

Acknowledgements

This work was supported by the National Research Foundation of Korea(NRF) grant funded by the Korea government(MSIT)(RS-2024-00352476).

Author contributions

K.-B. C., K.-S. J., and Y. S. R. designed the experiments. A. S. fabricated metal oxide semiconductor thin films and EGFET-based glucose sensors and analyzed the surface properties of the thin films and the electrical performance of EGFET-based devices. M. J. K. and D.-J. Y measured and analyzed the XPS spectra. S. K. and D. W. K. measured and analyzed the AFM. S. Kim, J. H. Bae, and S. Park measured and analyzed the TEM data. K.-S. J. and A. S. wrote the manuscript. All authors discussed the experimental results and commented on the manuscript. A. S. and M. J. K. wrote the revised manuscript as co-first author. All the authors have approved the final version of the manuscript.

Declarations

Competing interests

The authors declare no competing interests.

Additional information

Supplementary Information The online version contains supplementary material available at https://doi.org/10.1038/s41598-024-76885-x.

Correspondence and requests for materials should be addressed to Y.S.R., K.-S.J. or K.-B.C.